Multi-objective evolutionary algorithms for optimal scheduling
Wang, Y.

Citation
Wang, Y. (2022, January 19). *Multi-objective evolutionary algorithms for optimal scheduling*. Retrieved from https://hdl.handle.net/1887/3250350

Chapter 3

Diversity-based and Cone-based Multi-objective Evolutionary Algorithms

This chapter proposes an algorithm that will play an important role in solving multi-objective optimization problems of this thesis. The first part of this chapter is dedicated to answering RQ1, which is to develop an MOEA and compare it with state-of-the-art MOEAs. The proposed MOEA is called diversity indicator-based MOEA (DI-MOEA). DI-MOEA introduces a new principle to use non-dominated sorting combined with a set-based diversity indicator which can be efficiently computed, and it can achieve a uniformly distributed PF approximation regardless of the shape of the PF.

Followed by the introduction of several alternatives to Pareto dominance relationship in the previous chapter, the second part of this chapter aims to improve the performance of Pareto dominance by making use of its geometrical property, furthermore, propose an approach to promote the behavior of MOEAs in general (RQ2). The proposed cone order increases solutions' dominance area and the convergence speed of MOEAs adopting it. Special emphasis is given to many-objective optimization due to the degraded ability of Pareto dominance to establish a ranking when handling many-objective problems.

3.1   Diversity Indicator-based MOEAs

As mentioned before, indicator-based optimization has been a successful principle for MOEA design. The idea is to guide the search for approximating the Pareto front by a performance indicator. Ideally, the indicator captures both convergence to the Pareto front and a high diversity, and it does not require a priori knowledge of the Pareto front shape and location. It is, however, so far difficult to define indicators that scale well in computation time for high dimensional objective spaces, and that distribute points evenly on the Pareto front. Moreover, the behavior of commonly applied indicators depends on additional information, such as reference points or sets. For example, when the hypervolume indicator is used for performance comparison in indicator-based MOEAs, it has been show that the distribution of points is biased towards the knee point and the boundary if the reference point is not properly set [62]. Some multi-indicator-based MOEAs have been created to overcome these issues by using multiple quality indicators, such as [39], [40]. In this work, a diversity-indicator based multi-objective evolutionary algorithm is proposed. It combines principles from Pareto dominance-based approach and from indicator-based algorithms. Instead of requiring the indicator to take into account diversity and Pareto dominance, it is proposed to

- use dominance rank as a primary selection indicator, in order to ensure convergence to the Pareto front;

- use performance indicators that measure the diversity *of a set* of mutually non-dominated solutions.

However, as opposed to Pareto dominance-based approaches such as SPEA2 and NSGA-II that also maintain diversity, in DI-MOEA, the diversity of a set is measured by a scalar value, such that convergence to a maximum diverse set can be achieved and theoretically assessed.

Based on these principles, DI-MOEA therefore takes advantage of Pareto dominance-based approaches, and excludes the complex structure and parameters in decomposition-based and contemporary indicator-based approaches. Most importantly, experimental results show that it can find well converged and evenly spaced Pareto front approximations without the involvement of any reference points and assumptions about the location and shape of the Pareto front.

From here on, the adopted diversity indicator, i.e., the Euclidean distance based geometric mean gap indicator is introduced in detail. The proposed algorithm is

described and experimental results on benchmark problems are shown. Lastly, a conclusion of the work is given and some possible future work is indicated.

3.1.1   Diversity Indicators and Gap Contribution

There exist many indicators that assess the diversity of a distribution of points in $\mathbb{R}^m$. Among these, the Weitzman indicator and discrepancy measures have excellent theoretical properties, but their computation is expensive. The Hausdorff distance and related measures are indicators that would require the knowledge of the set on which points should be distributed, which is typically not available in Pareto optimization. The Solow-Polasky indicator has been suggested in the context of diversity assessment due to its moderate computational effort and good theoretical properties [105]. However, it is sensitive to the choice of the correlation strength parameter of an exponential kernel function and it requires matrix inversion which might cause numerical instability. The gap indicators (or the averages of distances to nearest neighbours) have been suggested in [37]. They are very fast to compute and easy to implement diversity indicators. In addition, they have certain favorable theoretical properties and empirical results show that their maximization results in diversified, evenly spread approximation sets. These results were obtained for multimodal optimization [124] and evolutionary level set approximation [74] for a wide range of test problems.

Let A define a set of points in $\mathbb{R}^m$, $D(x, A \setminus \{x\}) = \min_{a \in A \setminus \{x\}}\{d(x, a)\}$ and d denote the Euclidean distance, then the gap indicators (GI) are defined as follows:

$$GI_{\min}(A) = \min_{x \in A}\{D(x, A \setminus \{x\})\} \qquad \text{Minimal gap}$$

$$GI_{\Sigma}(A) = \frac{1}{|A|} \sum_{x \in A} D(x, A \setminus \{x\}) \qquad \text{Arithmetic mean gap}$$

$$GI_{\Pi}(A) = \left(\prod_{x \in A} D(x, A \setminus \{x\})\right)^{\frac{1}{|A|}} \qquad \text{Geometric mean gap.}$$

Note, that $GI_{\min}$ is the well known diversity indicator used in the max-min diversity problem [50]. One can leave out the exponent in GI_{Π} and this yields the product distance to the nearest neighbour (PDNN) indicator, considered by Wessing [124] in the context of multimodal optimization. Wessing [124] pointed out that GI_{Π} obtains the value of zero in case of duplicates in the set, a property that also holds for $GI_{\min}$. Besides, it can only be used for comparing sets of equal size. Since we are using the indicator contribution as a relative measure of performance of points, these two properties do not cause problems.

In indicator-based steady state selection [9] is to optimize a quality indicator QI for a solution set. W.l.o.g. we assume the quality indicator is to be maximized. The selection strategy is to add a non-dominated solution x to an approximation set A of size μ and then retain the best subset $S \subset P$ with $|S| = \mu$ of the new set $P = A \cup \{x\}$. This can be achieved by removing the point that contributes the least to the quality indicator. The indicator contribution of a point $p \in P$ is defined as:

$$\Delta_{QI}(p, P) \leftarrow QI(P) - QI(P \setminus \{p\}).$$

In DI-MOEA, the set-indicator contribution of the individual $p \in P$ is defined as the difference of the geometric mean gap indicator value of the set with the individual p minus the indicator-value of the set without it. The computation of the minimal contributor in case of the gap indicators can be solved by computing the solution to the all point nearest neighbour problem (APNN). The straightforward implementation, i.e. measuring distance between all pairs, requires a running time of $O(n^2)$. The APNN problem can be solved by Vaidya's algorithm [107] in optimal time $O(n \log n)$ for a fixed dimensional space and any Minkowski metric, including the Euclidean metric. The Euclidean distance is chosen as distance measure due to its rotational invariance.

3.1.2 Algorithm

A hybrid selection scheme: the $(\mu + \mu)$ generational selection operator and the $(\mu + 1)$ steady state selection operator, is utilized in DI-MOEA. The algorithm consists of two components:

- The $(\mu + \mu)$ generational selection operator: When the population is layered to multiple (more than one) dominance ranks, it indicates that the population has not yet converged to the true Pareto front. In this case, the $(\mu + \mu)$ generational selection operator is used to explore the decision space for dominating solutions. In this stage, a strict consideration of the diversity indicator is not yet the key determinant factor. Rather the first priority should be to push the population quickly to the Pareto front. Still, diversity is considered as a secondary ranking criterion in order to bring the points in a good starting position for searching for a uniformly distributed population. Overall, the selection operator is using non-dominated sorting as a primary ranking criterion, then if more than μ solutions are obtained by adding a layer, two alternative strategies are proposed

---

Algorithm 1 DI-MOEA

1: $P_0 \leftarrow init();$ //Initialize random population
2: $popsize \leftarrow |P_0|;$
3: $(R_1, ..., R_{\ell_0}) \leftarrow$ Partition P_0 into subsets of increasing dominance rank; //Non-dominated sorting
4: **for each** $i \in \{1, \ldots, \ell_0\}$ **do**
5:     calculate diversity indicator for all solutions based on the current front;
6: **end for**
7: $t \leftarrow 0;$
8: **while** Stop criterion not satisfied() **do**
9:     **if** $\ell_t > 1 \;||\; t == 0$ **then**
10:        // $(\mu + \mu)$ selection operator
11:        $Q_t \leftarrow Gen(P_t);$ // Generate offspring with the size of $popsize$ by variation
12:        Evaluate $Q_t;$
13:        $P_t = P_t \cup Q_t$ // Combine offspring and parents
14:        $(R_1, ..., R_{\ell_t}) \leftarrow$ Partition P_0 into subsets of increasing dominance rank; //Non-dominated sorting
15:        $i \leftarrow 0;$ $P_{t+1} \leftarrow \emptyset;$
16:        **while** $|P_{t+1}| < popsize$ **do**
17:            $P_{t+1} \leftarrow$ all solutions on i-th front $R_i;$
18:            $i \leftarrow i + 1;$
19:        **end while**
20:        **if** $|P_{t+1}| > popsize$ **then**
21:            $n \leftarrow |P_{t+1}| - popsize$
22:            **while** $n > 0$ **do**
23:                calculate diversity indicator for all solutions on the last front;
24:                remove the least contributor solution based on rank and diversity;
25:                $n \leftarrow n - 1;$
26:            **end while**
27:        **end if**
28:     **else**
29:        // $(\mu + 1)$ selection operator
30:        $q \leftarrow Gen(P_t);$ // Generate only an offspring by variation
31:        $P_t \leftarrow P_t \cup \{q\};$
32:        Rank P_t based on Pareto dominance rule; //Non-dominated sorting
33:        **for** each front **do**
34:            calculate set-indicator contribution for all solutions on the least ranked front $|R_{\ell_t}|$, if $|R_{\ell_t}| > 1;$
35:        **end for**
36:        remove the least contributor to diversity-indicator on the least ranked front;
37:     **end if**
38: **end while**

---

to truncate: the crowding distance (*variant 1*) as in NSGA-II, and the diversity indicator contribution (*variant 2*), where points are successively removed in a greedy manner and the contributions are recomputed after each removal. Under the condition that the μ selected solutions are mutually non-dominated after an iteration, the algorithm switches to the $(\mu + 1)$ steady state selection operator.

- The $(\mu+1)$ steady state selection operator: When the parent population consists of only one non-dominated set, it is likely that the population has already reached a region near the Pareto front. In this case, the indicator-based $(\mu + 1)$ steady state selection operator is applied, as described in Section 3.1.1. It discards the least contributor to the quality indicator, here, the diversity indicator. The intent is to achieve a uniformly distributed set on the Pareto front, that is to converge to a maximum of the diversity indicator. If there are more than one dominance ranks in the resulting population, the algorithm switches back to a $(\mu + \mu)$ generational selection operator.

Besides the hybrid selection scheme, another important design choice is the quality indicator, to be specific, the Euclidean distance based geometric mean gap indicator is used to guide the search towards the uniformly distributed Pareto front approximations regardless of the shape of the Pareto front. The proposed algorithm is presented as pseudo-code in Algorithm 1.

3.1.3   Experimental Results and Discussion

In this section, simulations are conducted to demonstrate the performance of the proposed algorithm. Because two different diversity measures are employed in the $(\mu + \mu)$ generational selection operator, two variants of DI-MOEA are involved in the experiments: the crowding distance and the set-indicator contribution are chosen as the second measure in the generational $(\mu + \mu)$ selection operator in algorithm DI-1 and algorithm DI-2 respectively.

In the simulations[1], the SBX operator with an index of 15 (30 in NSGA-III and a differential evolution operator is used in MOEA/D.) and polynomial mutation with an index 20 are used. The crossover and mutation probabilities are set to 1 and $1/L$ respectively and L is the number of variables. In NSGA-III, the number of

---

[1] All MOEAs in the thesis are implemented and tested based on the MOEA Framework (version 2.1, available from `http://www.moeaframework.org`). The MOEA Framework is Java-based framework for multi-objective optimization and it supports a number of MOEAs, test problems and search operators. It is also easy to be extended to introduce new problems and algorithms.

subdivisions is 99 for bi-objective problems, and 12 for tri-objective problems. The number of evaluation (NE) is chosen to be dependent on the complexity of the test problem. 20000 NE is used for ZDT problems and 100000 NE for DTLZ problems. The population size is 100 for all problems. Here we set the population size to be 100 because such number can be sufficient to represent the Pareto front of the adopted benchmark problems and it is an intuitive number usually given by the decision maker. However, for decomposition-based MOEAs, such as MOEA/D and NSGA-III, it is better to consider the number of reference vectors when specifying the population size. For example, the number of weight vectors in MOEA/D for three-objective problems is $1 + 2 + 3 + 4 + ... + H$ (where H is an integer), which is the same as the population size in MOEA/D. Thus, the population size of MOEA/D on three-objective problems can be 91 or 105 (instead of 100).

Experiments on bi-objective problems

For bi-objective problems, algorithms are tested on ZDT1, ZDT2 and ZDT3 with 30 variables. Two new algorithms, DI-1 and DI-2, are compared with NSGA-II, SMS-EMOA, NSGA-III and MOEA/D. Table 3.1 and Table 3.2 show the aggregate hypervolume and aggregate IGD across 30 independent runs (with a different seed for each run but same seeds for all algorithms). The aggregate value is the value obtained when the Pareto solutions from all runs are combined into one. For each problem in the two tables, the upper row denotes the aggregate hypervolume/IGD. (The best value is highlighted in bold.) The lower row is the standard deviation (Std) of results from 30 runs. The Mann-Whitney U test is used to determine if the medians of different algorithms for the same problem are significantly indifferent. In the tables, algorithms whose median performance is indifferent to the algorithm with the best aggregate performance are also highlighted. It can be observed that SMS-EMOA or NSGA-III can achieve the best hypervolume and the best IGD on all three problems, and the proposed DI-MOEA can obtain better hypervolume and IGD than NSGA-II and MOEA/D. In some instances, DI-MOEA can even get better hypervolume and IGD than NSGA-III or SMS-EMOA.

Experiments on tri-objective problems

For tri-objective problems, DTLZ1 with 7 variables, DTLZ2 with 12 variables and DTLZ7 with 22 variables are tested. Both DI-1 and DI-2 behave very well, and they are indifferent on the statistical significance of median performance of aggregate

3.1.   Diversity Indicator-based MOEAs

Table 3.1: The aggregate hypervolume (HV) on bi-objective problems.

HV Std ↘	NSGA-II	SMS-EMOA	NSGA-III	MOEA/D	DI-1	DI-2
ZDT1	0.66399	**0.66602**	0.66428	0.66029	0.66473	0.66491
	4.8379e-04	7.2331e-05	3.9507e-04	0.0028	3.5973e-04	2.8447e-04
ZDT2	0.33002	0.33265	**0.33266**	0.32849	0.33073	0.33141
	4.7756e-04	8.7207e-05	0.0086	0.0030	4.9232e-04	5.8483e-04
ZDT3	0.51600	0.51718	**0.51720**	0.51582	0.51623	0.51634
	3.9954e-04	0.0013	0.0010	0.0011	4.1969e-04	2.7955e-04

Table 3.2: The aggregate IGD on bi-objective problems.

IGD Std ↘	NSGA-II	SMS-EMOA	NSGA-III	MOEA/D	DI-1	DI-2
ZDT1	0.00163	**0.00039**	0.00168	0.00385	0.00116	0.00106
	2.6517e-04	1.9915e-05	8.2835e-04	0.0018	1.4110e-04	9.7026e-05
ZDT2	0.00202	0.00084	**0.00051**	0.00247	0.00159	0.00120
	2.1844e-04	1.0340e-04	0.0088	0.0014	2.1557e-04	2.4062e-04
ZDT3	0.00092	**0.00037**	0.00054	0.00190	0.00087	0.00092
	1.5809e-04	0.0100	0.0080	8.6720e-04	1.6713e-04	1.3157e-04

hypervolume and IGD. Statistical data averaging 10 runs per problem and algorithm are shown on Table 3.3 and Table 3.4. DI-1 beats all the algorithms on the aggregate hypervolume on all problems, and DI-2 also behaves better than other algorithms except for SMS-EMOA on DTLZ1. For IGD, the new algorithms perform the best on DTLZ1 and DTLZ2 problems. NSGA-II obtains the best IGD on DTLZ7, while IGD values of DI-1 and DI-2 are only slightly higher than NSGA-II on DTLZ7, but better than all other algorithms.

Table 3.3: The aggregate hypervolume (HV) on tri-objective problems.

HV Std ↘	NSGA-II	SMS-EMOA	NSGA-III	MOEA/D	DI-1	DI-2
DTLZ1	0.80605	0.80732	0.78400	0.80198	**0.80806**	**0.80645**
	0.0062	1.8738e-04	0.0179	0.0015	0.0013	6.1716e-04
DTLZ2	0.44263	0.45269	0.41915	0.42907	**0.45511**	**0.45489**
	0.0070	5.8698e-05	5.1471e-04	0.0031	0.0033	0.0014
DTLZ7	0.31064	0.24694	0.30624	0.30164	**0.31227**	**0.31339**
	0.0034	0.0038	0.0328	0.0055	0.0051	0.0137

To easily observe the results of algorithms, the results on the tri-objective problems are visualized. Figure 3.1 shows the Pareto front approximations of a typical run on DTLZ1. It can be observed that the solutions of NSGA-II and MOEA/D are not uniformly distributed, and there are several overlaps in the result of NSGA-III. While, SMS-EMOA and DI-MOEA can obtain evenly spaced solutions on the linear Pareto front.

Table 3.4: The aggregate IGD on tri-objective problems.

IGD / Std	NSGA-II	SMS-EMOA	NSGA-III	MOEA/D	DI-1	DI-2
DTLZ1	0.02149	0.02074	0.04266	0.02779	**0.01966**	**0.02381**
	0.0063	8.1450e-04	0.0159	0.0018	0.0017	0.0016
DTLZ2	0.02414	0.03415	0.05181	0.03902	**0.01799**	**0.01909**
	0.0047	0.0014	2.1056e-04	0.0026	0.0019	0.0030
DTLZ7	**0.01820**	0.09182	0.02381	0.041367	0.01826	0.02191
	0.0027	0.0020	0.2151	0.0867	0.0017	0.0944

Figure 3.2 shows the Pareto front approximations of a typical run on DTLZ2. For NSGA-III, we observed the same phenomenon: some solutions are overlapping or very close. The result of SMS-EMOA is distributed across the Pareto front with emphasis on the boundary and knee regions of the Pareto front. The results of the two DI-MOEA variants are uniformly distributed and evenly spaced on the Pareto front.

DI-MOEA also behaves well on the multimodal DTLZ7 problem, which has non-linear disconnected Pareto front regions. Figure 3.3 shows the results under 200 population size and 500000 NE.

When running the DI-MOEA, it can be observed that the population evolves towards the Pareto front at the initial stage (the first phase) using the generational selection operator. After a short period where the two selection operators alternate (the second phase), the steady state selection operator takes over and the population converges to a set with maximum diversity (the third phase). When the number of objectives becomes large, the third phase is more prominent than the previous two phases because it is more likely for solutions to be mutually non-dominated for a large objective number. In the runs conducted on tri-objective problems, the generational selection operator was applied around 100-200 iterations before it switched to the steady state selection operator for the first time. The intermittent alternating phase took about 20-50 iterations, and in most of the running time, the algorithm used the steady state selection operator and throughout this phase, only occasionally the algorithm switched back to generational selection operator for at most a single iteration. Overall, the first and the second phase took only a minor amount of the total running time.

It is worth noting that we observed dominance resistant solutions (DRSs) [54] occasionally on the linear Pareto front of DI-2 on DTLZ1 tri-objective problem; these are points that have a large contribution to diversity, but dominate only a very narrow region exclusively. It might be necessary to keep these "special solutions", but on the other side, they make the Pareto front approximation less evenly distributed. A
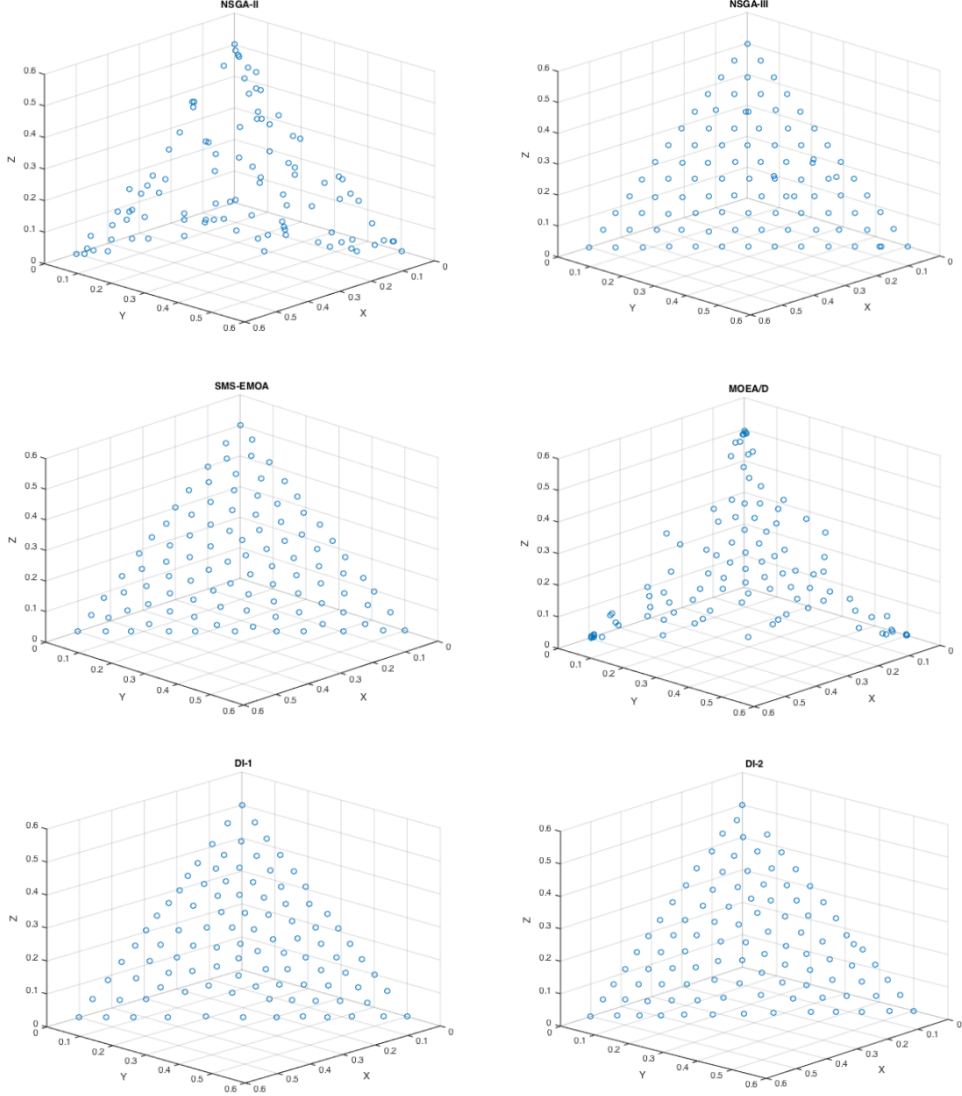
Figure 3.1: Representative Pareto front approximations of DTLZ1.

strategy has been tested to eliminate DRSs. Before the calculation of the set-indicator contribution for a front, each solution is checked by comparing with all other solutions: the distances between two solutions in all dimensions are calculated, if the result of the minimal distance divided by the maximal distance is too small, the current solution will be removed from the front. Therefore, a shrinked front is created and the diversity
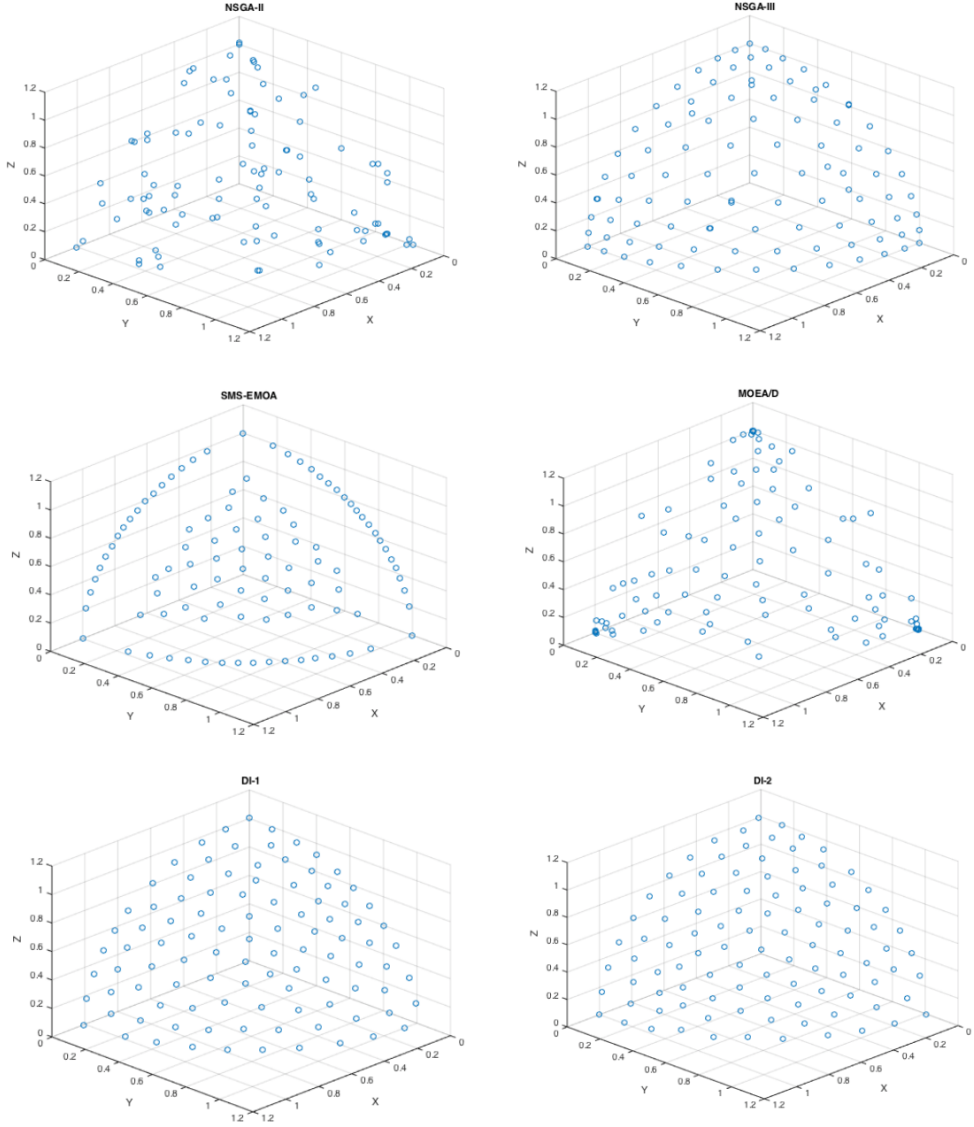
Figure 3.2: Representative Pareto front approximations of DTLZ2.

indicator can be calculated only in the new front. The underlying idea of this strategy is that for two solutions, if their distance is too close in one dimension and too large in another dimension, keeping both of them will result in an uneven distribution.
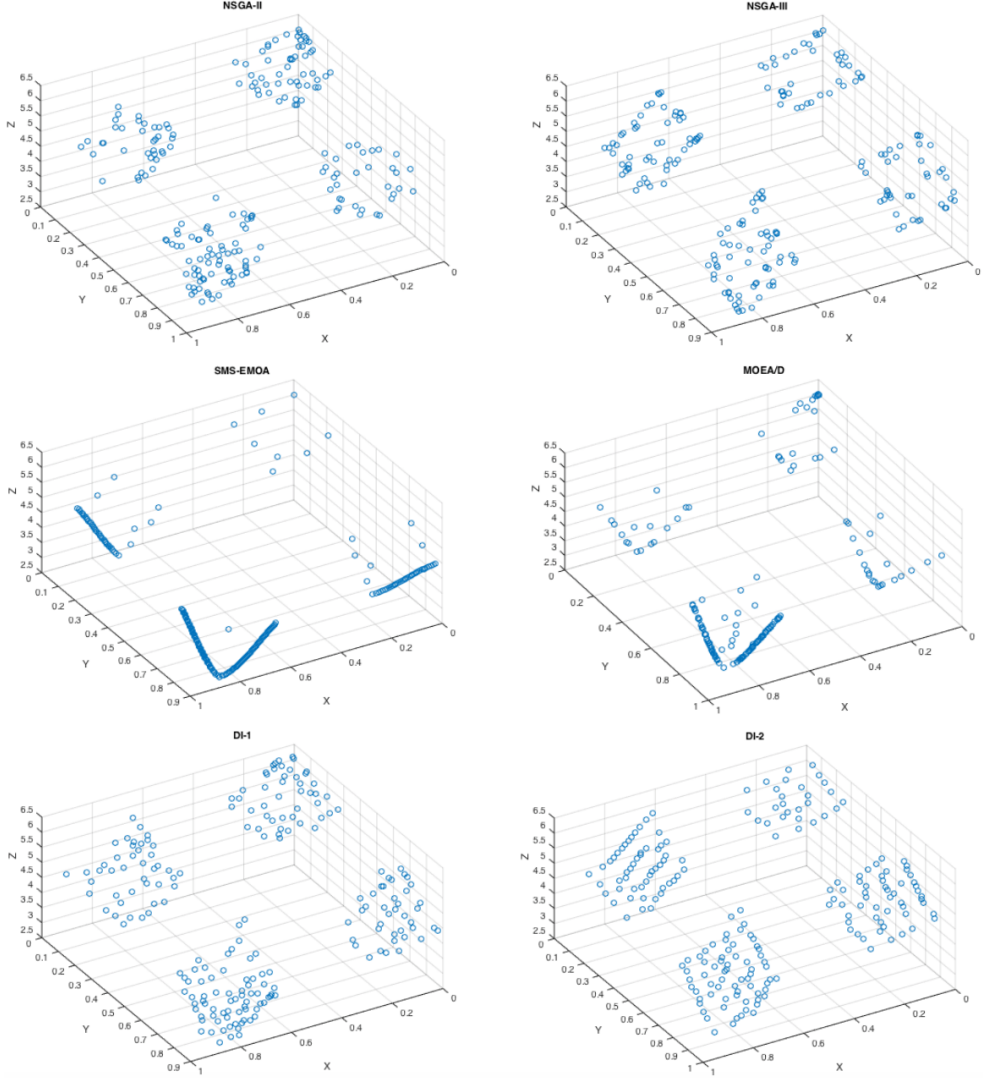
Figure 3.3: Representative Pareto front approximations of DTLZ7.

3.1.4 Conclusion and Further Work

The proposed DI-MOEA combines the advantage of Pareto dominance-based and indicator-based methods. Moreover, the achieved Pareto front approximations are excellent in both hypervolume indicator and IGD. In particular, the relative performance of DI-MOEA even gets better with an increasing number of objectives. The

set-indicator used in our algorithms is computationally simpler than the hypervolume indicator and only depends linearly on the number of objectives, making it possess a potential advantage on many-objective optimization problems. Most importantly, the uniformly distributed, evenly spaced solution set can be achieved without the use of decomposition sets and the estimation of the location and shape of the true Pareto front.

In the current implementation of DI-MOEA, only a naive way of calculating the Euclidean distance based geometric mean gap is implemented. Although the computational time of the implemented algorithm is shorter than SMS-EMOA, it should be further improved, e.g., by using Vaidya's algorithm [107] and incremental updates of contributions. Besides, DI-MOEA holds the promise of performing well in many-objective optimization. To study this, its performance should be tested on many-objective optimization benchmarks, paying special attention to effects that might occur in high dimensional objective spaces, such as distance concentration and the increasing number of non-dominated solutions.

3.2   Cone-based MOEAs

In this section, the edge-rotated cone order is first proposed for the purpose of building an ordering which can guide the search towards the Pareto front better than the Pareto order in MOEAs. Two different methods have been proposed to implement the edge-rotated cone order. Afterwards, the edge-rotated cone order is integrated in MOEAs by a proper approach which gives consideration to both convergence and diversity in the evolutionary searching process. The integrated MOEAs are then tested on multi-objective and many-objective optimization problems to compare with original MOEAs. Moreover, the ability of the edge-rotated cone order on expressing preferences in evolutionary multi-objective optimization is investigated.

3.2.1   Edge-rotated Cone Order

In an MOEA, if a solution can dominate more areas based on the adopted dominance relation, the algorithm is capable of exploring more solutions and hence accelerating convergence. To this end, the edge-rotated cone is devised by widening the angle of the Pareto order cone and it allows a solution to dominate a larger area. Given a linearly independent vector set $\{w_1, w_2, \ldots, w_m\}$, a cone can be generated in m-dimensional space.

Definition 3.1 (Generated m-dimensional cone)**.** The cone generated by the vectors $w_1, w_2, \ldots, w_m$ is the set $C = \{z : z = \lambda_1 w_1 + \lambda_2 w_2 + \cdots + \lambda_m w_m, \forall \lambda_1, \lambda_2, \ldots,$ $\lambda_m \geq 0, \lambda \neq 0\}$; $w_1, \ldots, w_m$ are linearly independent.

Figure 3.4 presents a two dimensional scenario of generating the standard Pareto order cone and edge-rotated cones. The Pareto order cone is the cone constructed by two half-lines aligned with two vectors, $\vec{a}$ and $\vec{b}$, which support an angle of $90°$. Similarly, vectors $\vec{L1}$ and $\vec{L2}$ determine a cone with an angle of $150°$. Intuitively, this cone can be formed by rotating the edges of the Pareto order cone towards the opposite direction around the origin. Note that vectors $\vec{L3}$ and $\vec{L4}$ determine a cone with an angle of $180°$ and the cone with an angle of $180°$ is a line. Any two vectors between $\vec{L3}$ and $\vec{L4}$ (excluding at least one of $\vec{L3}$ and $\vec{L4}$) can construct a convex cone (Definition 2.16), i.e., the space to the right of the corresponding lines and the lines themselves.
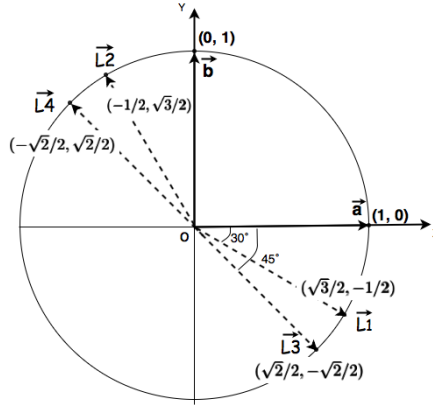
Figure 3.4: Cones with different angles.

When applying this cone order by means of the Minkowski sum (Definition 2.13), a solution can dominate more objective space. The left image of Figure 3.5 shows an example of applying the Pareto order cone to illustrate Pareto dominance relation, i.e., P dominates the points in $P \oplus \mathbb{R}^2_{\succ_o}$ and Q dominates the points in $Q \oplus \mathbb{R}^2_{\succ_o}$. Here, $\oplus$ is the Minkowski sum; $\mathbb{R}^2_{\succ_o}$ is equal to the cone constructed by $\vec{a}$ and $\vec{b}$ in Figure 3.4, the origin is excluded. In other words the non-negative quadrant with origin excluded.

It can be seen that P and Q are mutually non-dominated in terms of Pareto dominance relation because neither of them is in the dominating space of the other point. However, when an edge-rotated cone (e.g., the cone constructed by $\vec{L1}$ and $\vec{L2}$
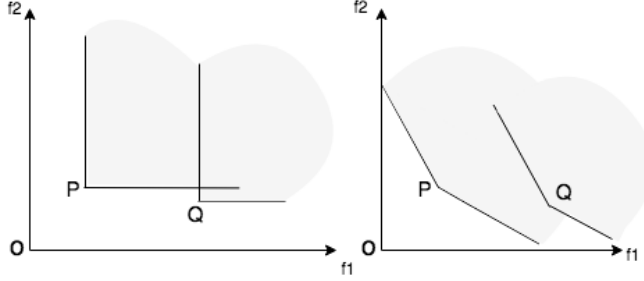
Figure 3.5: Pareto cone and edge-rotated cone orders.

in Figure 3.4) is adopted in the right image, the dominance relation between the point P and Q has changed and now Q is dominated by P.

The edge-rotated cone can be interpreted as a constraint on trade-offs. In Figure 3.5, two points $P = (p_1, p_2)$ and $Q = (q_1, q_2)$ are Pareto incomparable in $\mathbb{R}^2$. The trade-off, that is, the decrease in f_2 per unit of increase of f_1 is $\frac{p_2 - q_2}{q_1 - p_1}$. It is easily seen that in case $\frac{p_2 - q_2}{q_1 - p_1} \leq \tan(\alpha)$ (Here, α is the rotating angle on the edge of Pareto cone.), the points P and Q become comparable in the edge-rotated cone order and if $\frac{p_2 - q_2}{q_1 - p_1} > \tan(\alpha)$ the points P and Q stay incomparable in the edge-rotated cone order. Similarly, if for the decrease in f_1 per unit increase of f_2 it holds that $\frac{q_1 - p_1}{p_2 - q_2} \leq \tan(\alpha)$, then the points Q and P become comparable in the edge-rotated cone order and if $\frac{q_1 - p_1}{p_2 - q_2} > \tan(\alpha)$, then they are still incomparable in the edge-rotated cone order. In summary, if for two Pareto incomparable points one of the trade-offs is bounded by $\tan(\alpha)$, then the points are comparable in the edge-rotated cone order; in case, both trade-offs are bigger than $\tan(\alpha)$, the points are also incomparable with respect to the edge-rotated cone order.

When using the edge-rotated cone order in MOEAs, since the concave cones do not give rise to a strict partial order and the non-dominated points in the order generated by acute cones can be dominated in the Pareto order, the adopted edge-rotated cones are restricted to convex obtuse cones obtained by rotating each edge of the standard Pareto cone towards the outside with an angle of maximal $45°$. For example, in the case of a bi-objective problem, one edge of the cone can exist between $\vec{a}$ and $\vec{L3}$ and another edge of the cone can exist between $\vec{b}$ and $\vec{L4}$. The approach of widening the standard Pareto cone in m-dimensional space ($m > 2$) is the same. Each edge of the standard Pareto order cone is rotated around the origin by an angle of maximal $45°$ towards the opposite direction of the identity line in the first cube's orthant on the plane consisting of the edge and the identity line. In m-dimensional space, the identity

line in the first cube's orthant is the line that passes through the origin and the point $(1, ..., 1)$.

It is worth noting that solutions that are dominating in the Pareto order are also dominating in the edge-rotated cone order. Therefore, it is guaranteed that a minimal element of the edge-rotated cone order is also a minimal element of the Pareto order, and thus algorithms that converge to globally efficient points under the edge-rotated cone order will also converge to globally Pareto efficient points.
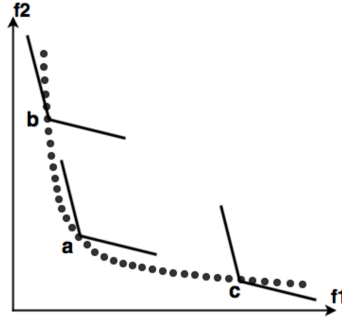
Figure 3.6: Trade-off on Pareto front.

The edge-rotated cone gives rise to an extended dominance relation and it establishes an ordering among Pareto incomparable solutions (i.e., being Pareto non-dominated to each other) in the sense that better Pareto incomparable solutions are preferred. By using the edge-rotated cone, a solution, especially the solution which is not in the knee region, has a higher chance to be dominated by other solutions. The knee region is the region where the maximum trade-off of objective functions takes place. For the Pareto front in Figure 3.6, the knee region is where the Pareto surface bulges the most, i.e., the region near solution a. When comparing the knee point a with another solution c, solution c has a better (i.e., lower) $f2$ value as compared to solution a. However, this small improvement leads to a large deterioration in the other objective $f1$. Due to the reason that in the absence of explicitly provided preferences, all objectives are considered equally important, solution a, thus, is more preferable than solution c. It has been argued in the literature that knee points are the most interesting solutions and preferred solutions [12, 13, 20, 24]. In this sense, although not all globally efficient points might be obtained by the edge-rotated cone orders, the edge-rotated cone orders naturally filter out non-preferred solutions. In Figure 3.6, when applying the edge-rotated cone, solutions in the knee region can survive, while

solutions like b and c are on the flat Pareto surface and are more easily to be dominated. The feature of the edge-rotated cone to eliminate solutions can be appreciated as an advantage especially in the realm of many-objective optimization considering the exponential increase in the number of non-dominated solutions necessary for approximating the entire Pareto front.

3.2.2   Implementation Methods

Two different methods have been proposed to implement the edge-rotated cone order. The first one emphasises on its geometrical property and the second one inclines towards its mathematical characteristic.

Method 1

Let us assume an edge-rotated cone constructed by $\vec{L1}$ and $\vec{L2}$ (Figure 3.4) is adopted in the right image of Figure 3.7. The area dominated by P can be determined by two lines: PA and PB. We can see that A is equal to $P + (\cos(-\alpha), \sin(-\alpha))$ and B is equal to $P + (\sin(-\alpha), \cos(-\alpha))$, where α is the rotated angle of the edge with respect to the standard Pareto order cone. In this example, α is $\pi/6$ (i.e., $30°$); the points A and B are then $P + (\sqrt{3}/2, -1/2)$ and $P + (-1/2, \sqrt{3}/2)$ respectively.
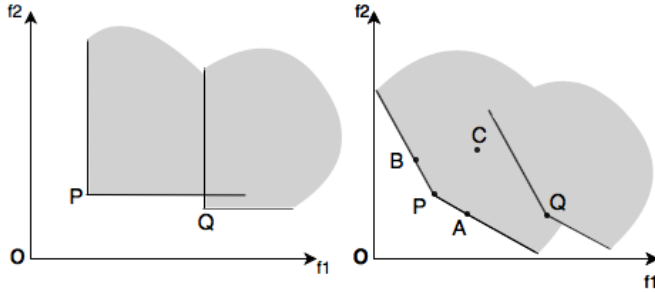
Figure 3.7: Pareto cone and edge-rotated cone orders.

In order to determine whether P dominates Q, we choose a point C on the identity line of the extension cone as a reference point which is known to be dominated by P. For instance, take C to be $P + (1, 1)$. To learn if another point Q is dominated by P or not, we only need to compare its position relative to the reference point, i.e., if Q and C are on the same side of line PA, and at the same time, both points are on the same side of line PB, Q is dominated by P.

Line PA can be defined by $ax + by + c = 0$, where the parameters, a, b and c, can be determined by two points on the line, i.e., P and A. To identify if two points, C and Q, are on the same side of this line, we only need to substitute these two points in $ax + by + c$, if the values of $ax + by + c$ are both negative or positive, it can be concluded that two points are on the same side of this line.

This comparison approach of identifying the dominance relationship between two points with the edge-rotated cone can also be easily implemented in larger dimensional space. When the number of objectives is m ($m > 2$), the space dominated by a point (e.g., P) is composed of m hyperplanes; each hyperplane is determined by m points and these m points include P and other $m - 1$ points picked from $(P_1, \ldots, P_i, \ldots, P_m)$ successively. The point P_i ($\in \mathbb{R}^m$) is equal to $P + o_i$; and the point o_i locates the new position of the ith edge of the cone together with the origin, the value of o_i is the ith column of the following ($m \times m$) matrix.

$$
\begin{bmatrix}
\cos(-\alpha) & \frac{\sin(-\alpha)}{\sqrt{m-1}} & \cdots & \frac{\sin(-\alpha)}{\sqrt{m-1}} \\
\frac{\sin(-\alpha)}{\sqrt{m-1}} & \cos(-\alpha) & \cdots & \frac{\sin(-\alpha)}{\sqrt{m-1}} \\
\vdots & \vdots & \ddots & \vdots \\
\frac{\sin(-\alpha)}{\sqrt{m-1}} & \frac{\sin(-\alpha)}{\sqrt{m-1}} & \cdots & \cos(-\alpha)
\end{bmatrix}
\tag{3.1}
$$

The equation of a hyperplane in the m-dimensional space is $a_1 x_1 + a_2 x_2 + \cdots + a_i x_i + \cdots + a_m x_m + a_{m+1} = 0$, where x_i ($i \in (1, \ldots, m)$) is the ith objective value and a_i ($i \in (1, \ldots, m + 1)$) is the parameter. All parameters of the hyperplane (i.e., from a_1 to a_{m+1}) can be calculated by the m points on the hyperplane. Again, the point C (i.e., $P + (1, \ldots, 1)$) can be used as the reference and if another point Q is dominated by P, the two points Q and C would be on the same side of all hyperplanes, meaning that if for each hyperplane, we put the two points in the equation $a_1 x_1 + a_2 x_2 + \cdots + a_i x_i + \cdots + a_m x_m + a_{m+1}$, both results would be negative or positive.

Method 2

In this method, a criterion is derived by which one can determine whether a point $Q \in \mathbb{R}^2$ is dominated by a point $P \in \mathbb{R}^2$ with respect to the edge-rotated cone order. Let $e_1 := \begin{bmatrix} 1 \\ 0 \end{bmatrix}$ and $e_2 := \begin{bmatrix} 0 \\ 1 \end{bmatrix}$ be the edges of the two-dimensional standard Pareto cone. Then the edges of the edge-rotated cone by a rotation angle α ($0 \leq \alpha \leq \frac{\pi}{4}$) are Ae_1 and Ae_2, where $A = \begin{bmatrix} \cos(-\alpha) & \frac{\sin(-\alpha)}{\sqrt{2-1}} \\ \frac{\sin(-\alpha)}{\sqrt{2-1}} & \cos(-\alpha) \end{bmatrix}$.

A point Q lies in the edge-rotated cone region of P if and only if for some λ, $Q = P + \lambda_1 A e_1 + \lambda_2 A e_2$ such that $\lambda_1, \lambda_2 \geq 0, \lambda \neq 0$. This is equivalent to: for some λ, $A^{-1}(Q - P) = \lambda_1 e_1 + \lambda e_2$ such that $\lambda_1, \lambda_2 \geq 0, \lambda \neq 0$. In short, *P dominates Q with respect to the edge-rotated cone order if and only if the components of $A^{-1}(Q-P)$ are non-negative and at least one of them is strictly positive.* Thus, once the inverse matrix of A is computed $(A^{-1} = c \cdot \begin{bmatrix} \cos(\alpha) & \sin(\alpha) \\ \sin(\alpha) & \cos(\alpha) \end{bmatrix}, c := \frac{1}{(\cos(\alpha))^2 - (\sin(\alpha))^2})$, it can readily be determined whether Q is in the dominating region of P. Moreover, in case the components are non-zero and have opposite signs, then the points are incomparable. In case the components are non-positive and at least one of them negative, then Q dominates P.

The approach can easily be applied to three or many objective problems. When the number of objectives is m $(m > 2)$ and the rotation angle for each edge of the cone is α, the $(m \times m)$ matrix (3.1) gives the coordinates of the unit point on rotated edges: for each unit point on the edge of the standard Pareto cone, each column of the matrix gives its new coordinates after rotation. For example, in three-dimensional space, (1, 0, 0) is the unit point on one edge of the standard Pareto cone, then $(\cos(-\alpha), \frac{\sin(-\alpha)}{\sqrt{2}}, \frac{\sin(-\alpha)}{\sqrt{2}})$ are its new coordinates after the edge is rotated by an angle of α $(0 \leq \alpha \leq \frac{\pi}{4})$.

When using the edge-rotated cone order in MOEAs by this method, the inverse matrix only needs to be calculated once and this leads to almost no extra computing time added in MOEAs.

3.2.3   Integration Algorithm

In a multi-objective optimization algorithm, by using the edge-rotated cone, a solution has a higher chance to be dominated by other solutions and thus the selection pressure toward the Pareto front is increased. However, an edge-rotated cone can degrade the diversity to some extent because more solutions will be dominated and therefore excluded from the result set. To circumvent this, Algorithm 2 is proposed to pick a proper cone order (the standard Pareto cone order or edge-rotated cone order) in each iteration of the algorithm in order to promote diversity in addition to convergence. Specifically speaking, at the beginning of each iteration, the population is ranked based on the current cone order; the edge-rotated cone order will be adopted only under the condition that all the solutions in the population are mutually non-dominated. In case the current population consists of multiple layers, the standard Pareto cone (i.e., the rotation angle is $0°$) is picked to select offspring. The underlying idea is when all
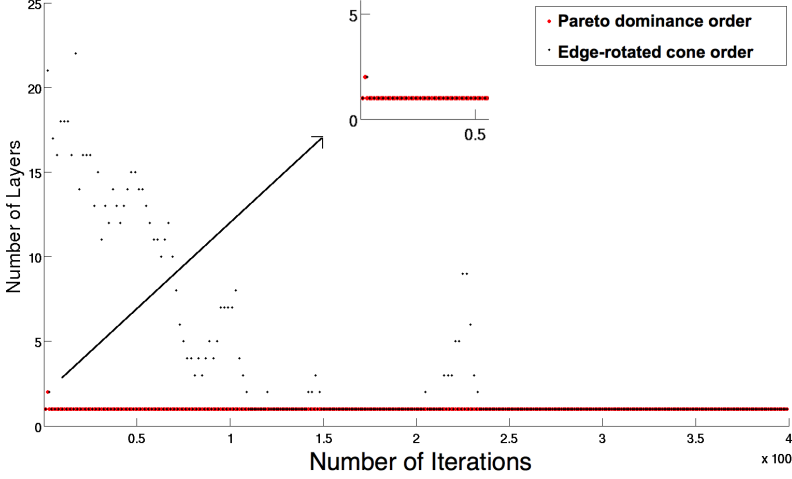
Figure 3.8: The dynamics of the number of layers.

the solutions are non-dominated with each other, the edge-rotated cone is adopted to enhance the selection pressure; otherwise, the standard Pareto cone is used to maintain the diversity of the population.

Algorithm 2 Applying a proper cone order in each iteration.

1: $m \leftarrow$ the number of objectives;
2: $Degree[m]$; // the rotation angle for each edge of the standard Pareto order;
3: $n\_rank \leftarrow$ Pareto rank number of current population;
4: **if** $n\_rank = 0$ **then**
5:      **for each** $i \in \{1, \ldots, m\}$ **do**
6:          $Degree[i] \leftarrow \pi/6$; // rotation angle is 30°
7:      **end for**
8: **else**
9:      **for each** $i \in \{1, \ldots, m\}$ **do**
10:          $Degree[i] \leftarrow 0$; // standard Pareto cone
11:      **end for**
12: **end if**

The ability of the edge-rotated cone to make Pareto incomparable solutions comparable can especially benefit many-objective optimization due to the reason that the likelihood of solution pairs of being comparable decreases exponentially with the increase of the dimension m. For many-objective optimization, a large portion of points in the objective space is non-dominated and the optimization process tends to produce

a large set of alternative solutions.

When Algorithm 2 is applied in NSGA-II on the DTLZ1 eight objective problem, Figure 3.8 compares the changes of the number of layers between running NSGA-II using only the Pareto dominance and involving the edge-rotated cone order with a rotation angle of 20° within the first 400 iterations (Population size is 100.). When running the original NSGA-II, except that one point lies at level 2 (i.e., the number of fronts is two) at the very beginning, the number of layers always remains one, meaning that all solutions in the current population are non-dominated with each other. As a result, the Pareto dominance relation has no effect on parent selection. That is, an individual with a larger crowding distance is always chosen as a parent in the binary tournament selection since all solutions have the same rank. In this manner, the selection pressure toward the Pareto front is severely weakened. However, when the edge-rotated cone is involved, the layering of the population is very noticeable. In this case, an ordering among the incomparable solutions is established and it can guide the search towards the Pareto front better.

3.2.4   Experimental Results

The proposed strategy can be integrated with any standard MOEA which works with a population in each iteration and uses the Pareto dominance relation to select solutions, such as NSGA-II [29], DI-MOEA [116], NSGA-III [26] and others. In this section, the edge-rotated cone order is applied by Algorithm 2 to observe its behavior on multi-objective and many-objective optimization problems respectively. To this end, different rotation angles have been tested, hypervolume and IGD have been adopted to compare the performance of the algorithms. The population size is 100 for all experiments.

Multi-objective Optimization

For starts, four tri-objective optimization problems have been chosen in the experiments, which are DTLZ1, DTLZ2, DTLZ7 and DTLZ2_convex. The first three problems are from the DTLZ problem test suite. The optimal Pareto front of DTLZ1 lies on a linear hyperplane. The optimal Pareto front of DTLZ2 is concave. DTLZ7 is a multi-modal problem. To measure the performance on the multi-objective optimization problem with a convex Pareto front, original DTLZ2 problem is transformed to DTLZ2_convex problem by simply decreasing all objective values by 3.5. When calculating the hypervolume of the solution set, the reference point is the point (0.6,

0.6, 0.6) for DTLZ1, the point (1.1, 1.1, 1.1) is the reference point for DTLZ2, the point (5, 5, 5) for DTLZ2_convex, and (1, 1, 6.5) for DTLZ7. Meanwhile, the origin is used as the ideal point. When calculating the IGD value, the reference sets of DTLZ1, DTLZ2 and DTLZ7 are from the MOEA framework, and the reference set of DTLZ2_convex is obtained by running DI-MOEA because DI-MOEA is good at achieving well-distributed solution sets. The merged non-dominated solution sets from 30 independent runs are used as the reference sets of DTLZ2_convex.

Firstly, the edge-rotated cone order is integrated by Algorithm 2 with NSGA-II which is one of the most popular Pareto dominance-based MOEAs. Regarding to the computing budget, when the number of evaluations is 30000, Table 3.5 shows the mean hypervolume and mean IGD from 30 independent runs when several different edge-rotated cone orders are adopted. The "P_cone" column provides the results obtained by the original MOEAs, i.e., the algorithms only adopt the standard Pareto order. The "30°" column gives the results of the algorithm involving the edge-rotated cone and each edge of the standard Pareto order cone has been rotated by 30°, and similar remarks are used for the remaining columns. The mean hypervolume and mean IGD values obtained by the original NSGA-II have been used as the reference values (printed in blue) to be compared with the results achieved by the algorithms involving the edge-rotated cone orders. For the algorithms combining the edge-rotated cones, the mean hypervolume and mean IGD values better than the values obtained by the original MOEAs have been highlighted in bold (i.e., a larger hypervolume value and lower IGD value); and the largest value for each algorithm among them is printed in red. At the same time, the standard deviation of each algorithm is also given under each mean hypervolume and mean IGD.

It can be observed that the performance of NSGA-II (for both the hypervolume and IGD values) can always be improved when the edge-rotated cone with a proper angle is involved, for example, when the rotation angle is 6° or 2°. However, the best performance takes place with different edge-rotated cones for different problems. When the rotation angle is 30°, the algorithm behaves the best on DTLZ1 problems and the rotation angle of 6° is the best on other problems. The standard deviations show the stable behavior of the algorithm involving the edge-rotated cone order, which is even better than the original NSGA-II.

When different edge-rotated cone orders are integrated in NSGA-III, Table 3.6 presents the mean hypervolume and mean IGD. NSGA-III is an extension of NSGA-II and it eliminates the drawbacks of NSGA-II such as the lack of a good diversity in a set of non-dominated solutions. Although NSGA-III is a decomposition-based MOEA,

Table 3.5: The mean hypervolume (M-HV) and mean IGD (M-IGD) when integrating edge-rotated cone orders with NSGA-II.

Problems	Metrics	P_cone	30°	12°	6°	2°
DTLZ1	M-HY	0.7064	**0.8621**	**0.8569**	**0.8490**	**0.8360**
	std	0.2731	0.0029	0.0143	0.0429	0.1111
	M-IGD	0.2420	**0.0676**	**0.0732**	**0.0807**	**0.0927**
	std	0.3102	0.0039	0.0168	0.0428	0.1194
DTLZ2 concave	M-HY	0.5276	0.2786	**0.5487**	**0.5399**	**0.5348**
	std	0.0044	0.0246	0.0029	0.0026	0.0031
	M-IGD	0.0709	0.4909	0.0801	**0.0674**	**0.0692**
	std	0.0034	0.0627	0.0040	0.0032	0.0028
DTLZ2 convex	M-HY	0.6862	0.4895	**0.6891**	**0.6921**	**0.6894**
	std	0.0030	0.0010	0.0018	0.0019	0.0025
	M-IGD	0.0707	0.3490	0.0835	**0.0706**	**0.0698**
	std	0.0030	0.0012	0.0026	0.0026	0.0032
DTLZ7	M-HY	0.2739	0.0151	0.2716	**0.2787**	**0.2767**
	std	0.0016	0.0000	0.0009	0.0019	0.0013
	M-IGD	0.0519	0.9587	0.1213	**0.0482**	**0.0492**
	std	0.0029	0.0001	0.0023	0.0029	0.0028

the basic framework of NSGA-III is similar to NSGA-II. It employs non-dominated sorting to partition the population into a number of fronts, but replaces the crowding distance operator with a clustering operator based on a set of reference points. NSGA-III is assumed to be powerful enough to handle these benchmark problems, however, according to the data in Table 3.6, it can be seen that its performance can still be improved by the edge-rotated cone order.

The same pattern can be observed from the two tables: the 30° rotation angle works best for DTLZ1 problem; a small rotation angle (i.e., 6° or 2°) works best for other problems, and a small rotation angle can almost always improve the behavior of the original algorithms. From the two tables, it can also be observed that the edge-rotated cone order can benefit NSGA-II more than NSGA-III. In some cases, the performance of NSGA-II with an edge-rotated cone can even reach the performance of the original NSGA-III.

A straightforward way to improve the results of MOEAs is to increase the computing budget. When the computing budget of the original MOEAs is increased to 300000, Table 3.7 gives the values of the mean hypervolume and mean IGD of NSGA-

Table 3.6: The mean hypervolume (M-HV) and mean IGD (M-IGD) when integrating edge-rotated cones with NSGA-III.

Problem	Metrics	P_cone	30°	12°	6°	2°
DTLZ1	M-HY	0.8709	**0.8771**	**0.8763**	**0.8756**	**0.8761**
	std	0.0108	0.0010	0.0015	0.0047	0.0013
	M-IGD	0.0616	**0.0538**	**0.0539**	**0.0552**	**0.0539**
	std	0.0224	0.0006	0.0006	0.0067	0.0004
DTLZ2	M-HY	0.5593	0.2628	0.5526	**0.5595**	**0.5600**
concave	std	0.0006	0.0159	0.0010	0.0007	0.0003
	M-IGD	0.0554	0.5353	0.0804	**0.0534**	**0.0554**
	std	0.0005	0.0522	0.0030	0.0008	0.0004
DTLZ2	M-HY	0.6941	0.4827	0.6823	0.6913	**0.6946**
convex	std	0.0024	0.0039	0.0025	0.0023	0.0023
	M-IGD	0.0635	0.3541	0.0898	0.0711	0.0641
	std	0.0028	0.0035	0.0041	0.0030	0.0027
DTLZ7	M-HY	0.2264	0.0697	0.2234	**0.2324**	**0.2288**
	std	0.0343	0.0496	0.0310	0.0352	0.0360
	M-IGD	0.3705	0.7702	0.4024	**0.3472**	**0.3614**
	std	0.2070	0.1296	0.1819	0.2085	0.2172

II and NSGA-III. It can be observed that the algorithms combining the edge-rotated cone order when only using a small computing budget can even behave better than the original NSGA-II and NSGA-III when using a large computing budget. Only in several cases (values in blue), the algorithm involving the edge-rotated cone order with the small budget cannot reach the performance of the original MOEAs with the large budget, but their behavior is already very close to the original MOEAs with the large budget.

Many-objective Optimization

In this section, four, six, eight objective DTLZ1, DTLZ2, DTLZ2_convex problems, UF11 and UF13 [136] have been chosen in the experiments. UF11 is a rotated instance of the 5D DTLZ2 test problem, and UF13 is the 5D WFG1 test problem. For each problem, the computing budget for running the algorithm (i.e., the number of evaluations) is determined by $\max\{100000, 10000 \times D\}$, where D is the number of decision variables. Likewise, hypervolume and IGD have been adopted to compare the performance of the algorithms. When calculating HV, the objective values of the

Table 3.7: The Mean hypervolume (M-HV) and mean IGD (M-IGD) of original NSGA-II and NSGA-III with larger computing budget.

Problem	DTLZ1	DTLZ2_concave	DTLZ2_convex	DTLZ7
M-HY	0.8630	0.5281	0.6884	0.2755
M-IGD	0.0657	0.0705	0.0698	0.0506
M-HY	0.8757	0.5603	0.6944	0.2284
M-IGD	0.0597	0.0552	0.0628	0.3599

reference point are 0.6 on DTLZ1, 1.1 on DTLZ2, 5 on DTLZ2_convex, 2.2 on UF11 and 11 on UF13. The origin is used as the ideal point. When calculating the IGD value, the merged non-dominated solution sets from all runs are used as the reference sets of the DTLZ2_convex problems and the reference sets of other problems are from the MOEA framework.

Tables 3.9 - 3.11 show the mean hypervolume and mean IGD from 15 independent runs when different edge-rotated cone orders are integrated in NSGA-II, DI-MOEA and NSGA-III. Similarly, for the algorithms combining the edge-rotated cone, the mean hypervolume and mean IGD values are better than the values obtained by the original MOEAs have been highlighted in bold; the largest respectively lowest value for each algorithm among them is printed in red. Tables for the DTLZ benchmark problems consist of four parts, namely four objective, six objective, eight objective with full budget, and eight objective with half budget. Both UF11 and UF13 are five objective problems and their behaviors with full budget and half budget are given in Table 3.11.

The following conclusions can be drawn from the data in these tables.

1. The algorithms do not work well when a large rotation angle is adopted (e.g., $30°$).

2. The algorithms show similar performance to the original MOEAs when the rotation angle is very small (e.g., $3°$).

3. When an intermediate rotation angle is adopted, the performance of the algorithms (both hypervolume and IGD values) shows a significant improvement except for a few cases which display values close to the original MOEAs.

4. Although it differs depending on the specific problems, the best performance is usually obtained when the rotation angle is $15°$.

5. It can be seen that the edge-rotated cone can improve the performance of all

three adopted MOEAs (i.e., NSGA-II, DI-MOEA and NSGA-III) in most cases when an intermediate rotation angle is used. Even though NSGA-III is assumed to be powerful enough to handle these benchmark problems, its performance can still be improved by the edge-rotated cone approach.

6. The edge-rotated cone can benefit MOEAs even more with the increase of the number of objectives. For example, when a 15° rotation angle is applied on the DTLZ2 (concave) four objective problem, the hypervolume of NSGA-II is improved from 0.5953 to 0.6760; for the six objective problem, the hypervolume is improved from 0.1224 to 0.8156; and for the eight objective problem, the hypervolume is improved from 0.0168 to 0.8850.

7. The edge-rotated cone can benefit the algorithm with a small computing budget more than the algorithm with a large budget. For example, when using half of the computing budget on UF13 five objective problem and the rotation angle is set to 20°, the hypervolume values of the Pareto fronts from NSGA-II, DI-MOEA and NSGA-III can be improved to 0.7259, 0.7254, 0.7073, which are already larger than the hypervolume values obtained by the original MOEAs with full budget, namely 0.6937, 0.6611 and 0.6497.

8. Even though the median values of the hypervolume and IGD values have not been presented in the tables, they show similar values as the mean values. At the same time, the standard deviations show a stable behavior of the edge-rotated cone order when it is integrated in MOEAs.

Preference-based Multi-objective Optimization

In the previous experiments, the rotation angles on all edges of the Pareto cone are kept the same. However, the edge-rotated cone is not necessarily "symmetric". When rotating the different edges of the Pareto cone by different angles, the generated edge-rotated cone can lead the search towards different focuses on the Pareto front. To observe the effect of the "unsymmetrical" edge-rotated cone, it is integrated in DI-MOEA and the tri-objective DTLZ2 concave and convex problems are adopted to observe the experimental results due to the typical shape of their Pareto fronts. The setting of the other parameters, such as the number of evaluations, population size, is the same as in previous experiments for multi-objective optimization.

The two left images in Figure 3.9 show the results of only rotating one edge of the cone on the concave DTLZ2 problem. The black points give the entire Pareto front

Table 3.8: The mean hypervolume (M-HV) and mean IGD (M-IGD) on DTLZ1.

Algorithms	Metrics	P_cone	30°	20°	15°	10°	6°	3°
Four objective (NE = 100000)								
NSGA-II	M-HV	0.5811	**0.7735**	0.9405	0.9403	0.9400	0.9393	0.9398
	std	0.3347	0.1918	0.0024	0.0021	0.0026	0.0021	0.0018
DI-MOEA	M-HV	0.4842	0.0000	**0.9535**	0.9537	0.9521	0.9538	0.9533
	std	0.4250	0.0000	0.0010	0.0009	0.0056	0.0005	0.0009
NSGA-III	M-HV	0.9447	0.6399	**0.9448**	0.9444	0.9458	0.9453	0.9452
	std	0.0024	0.2561	0.0020	0.0024	0.0020	0.0018	0.0028
NSGA-II	M-IGD	0.9725	**0.3083**	0.1537	0.1550	0.1553	0.1491	0.1511
	std	0.0044	0.0444	0.0036	0.0026	0.0037	0.0046	0.0034
DI-MOEA	M-IGD	1.2772	763.0901	0.1287	0.1287	0.1329	0.1303	0.1311
	std	1.4694	9.6585	0.0021	0.0026	0.0128	0.0019	0.0027
NSGA-III	M-IGD	0.1300	0.4122	**0.1297**	0.1295	0.1315	**0.1298**	0.1313
	std	0.0024	0.2506	0.0038	0.0031	0.0029	0.0027	0.0032
Six objective (NE = 100000)								
NSGA-II	M-HV	0.0000	0.0000	0.9857	0.9851	0.9844	0.9808	0.8922
	std	0.0000	0.0000	0.0007	0.0007	0.0010	0.0023	0.2001
DI-MOEA	M-HV	0.0000	0.0000	0.9911	0.9911	0.9906	0.9885	0.9728
	std	0.0000	0.0000	0.0002	0.0003	0.0002	0.0019	0.0084
NSGA-III	M-HV	0.9880	0.0000	0.9887	0.9885	0.9883	0.9881	0.9883
	std	0.0009	0.0000	0.0005	0.0006	0.0005	0.0008	0.0006
NSGA-II	M-IGD	75.4078	744.6850	**0.3041**	0.3026	0.3079	0.3256	0.4541
	std	41.1790	49.7971	0.0169	0.0136	0.0183	0.0159	0.2359
DI-MOEA	M-IGD	349.0537	769.4755	**0.3086**	0.3102	0.3151	0.3196	0.3791
	std	76.0015	37.4396	0.0050	0.0043	0.0064	0.0104	0.0291
NSGA-III	M-IGD	0.2990	770.0300	**0.2935**	0.3007	0.3020	0.3015	0.3020
	std	0.0101	40.8585	0.0050	0.0085	0.0095	0.0085	0.0092
Eight objective (NE = 120000)								
NSGA-II	M-HV	0.0000	0.0000	0.9957	0.9956	0.9937	0.9422	0.7397
	std	0.0000	0.0000	0.0003	0.0004	0.0005	0.1638	0.3584
DI-MOEA	M-HV	0.0000	0.0000	0.9976	0.9976	0.9965	0.8700	0.2850
	std	0.0000	0.0000	0.0001	0.0002	0.0007	0.2892	0.3758
NSGA-III	M-HV	0.9877	0.0000	0.9855	0.9858	0.9853	0.9865	0.9854
	std	0.0025	0.0000	0.0027	0.0038	0.0032	0.0042	0.0025
NSGA-II	M-IGD	128.0384	721.0803	**0.4286**	0.4272	0.4452	0.5575	0.8845
	std	56.8022	57.7441	0.0199	0.0148	0.0232	0.2231	0.4798
DI-MOEA	M-IGD	517.2231	758.8918	**0.4843**	0.4866	0.5043	0.8457	3.3619
	std	108.7324	142.8642	0.0068	0.0056	0.0106	0.6234	3.5900
NSGA-III	M-IGD	0.3599	418.6033	**0.3461**	0.3567	0.3565	0.3557	0.3594
	std	0.0113	43.8714	0.0106	0.0106	0.0123	0.0192	0.0096
Eight objective - Half budget (NE = 60000)								
NSGA-II	M-HV	0.0000	0.0000	0.9954	0.9944	0.7331	0.2971	0.2048
	std	0.0000	0.0000	0.0006	0.0012	0.3764	0.3660	0.3120
DI-MOEA	M-HV	0.0000	0.0000	**0.9634**	0.9972	0.9861	0.7335	0.0745
	std	0.0000	0.0000	0.0863	0.0003	0.0341	0.3592	0.1555
NSGA-III	M-HV	0.9813	0.0000	0.9855	0.9842	0.9849	0.9856	0.9863
	std	0.0138	0.0000	0.0027	0.0033	0.0033	0.0034	0.0027
NSGA-II	M-IGD	170.7728	681.8762	0.4248	0.4248	1.0092	2.3994	3.2542
	std	92.0427	64.1913	0.0204	0.0151	0.8559	2.0576	3.1045
DI-MOEA	M-IGD	592.0768	747.5064	**0.5889**	0.4881	0.5406	1.2579	4.0558
	std	93.9853	94.6608	0.2782	0.0087	0.0983	1.1140	2.8857
NSGA-III	M-IGD	0.3777	405.6668	**0.3509**	0.3576	0.3635	0.3663	0.3627
	std	0.0588	48.9879	0.0192	0.0107	0.0124	0.0216	0.0169

Table 3.9: The mean hypervolume (M-HV) and mean IGD (M-IGD) on DTLZ2 (concave).

Algorithms	Metrics	P_cone	30°	20°	15°	10°	6°	3°
Four objective (NE = 130000)								
NSGA-II	M-HV	0.5953	0.1971	0.5458	**0.6760**	**0.6525**	**0.6388**	**0.6333**
	std	0.0089	0.1182	0.0535	0.0041	0.0048	0.0080	0.0077
DI-MOEA	M-HV	0.6471	0.0913	0.5639	**0.6944**	**0.6897**	**0.6755**	**0.6688**
	std	0.0094	0.0012	0.0406	0.0038	0.0026	0.0066	0.0039
NSGA-III	M-HV	0.6597	0.2508	0.5749	**0.6863**	**0.6821**	**0.6652**	0.6592
	std	0.0054	0.1265	0.0362	0.0017	0.0040	0.0031	0.0066
NSGA-II	M-IGD	0.1634	0.8352	0.4037	0.1867	**0.1492**	**0.1536**	**0.1542**
	std	0.0045	0.2290	0.0794	0.0056	0.0040	0.0055	0.0041
DI-MOEA	M-IGD	0.1363	1.0405	0.3810	0.1731	**0.1264**	**0.1295**	**0.1279**
	std	0.0045	0.0183	0.0661	0.0049	0.0022	0.0061	0.0028
NSGA-III	M-IGD	0.1501	0.7553	0.3510	0.1749	**0.1361**	**0.1477**	**0.1490**
	std	0.0046	0.2196	0.0705	0.0039	0.0034	0.0054	0.0026
Six objective (NE = 150000)								
NSGA-II	M-HV	0.1224	0.0000	**0.4304**	**0.8156**	0.7608	0.7284	0.6490
	std	0.0701	0.0000	0.0254	0.0036	0.0067	0.0119	0.0221
DI-MOEA	M-HV	0.0000	0.0000	**0.4488**	**0.8397**	0.8016	0.7479	0.6543
	std	0.0000	0.0000	0.0126	0.0055	0.0055	0.0117	0.0347
NSGA-III	M-HV	0.8052	0.0000	0.4411	**0.8446**	0.8185	0.8127	0.8111
	std	0.0076	0.0000	0.0130	0.0048	0.0038	0.0056	0.0041
NSGA-II	M-IGD	0.7278	2.5612	0.7003	**0.3447**	**0.2856**	0.2887	0.3137
	std	0.0758	0.0090	0.0380	0.0119	0.0051	0.0046	0.0091
DI-MOEA	M-IGD	1.9390	2.5824	**0.6961**	0.2913	**0.2774**	0.2898	0.3335
	std	0.3246	0.0059	0.0285	0.0074	0.0026	0.0058	0.0172
NSGA-III	M-IGD	0.3125	2.5596	0.7260	0.3073	**0.3061**	0.3092	0.3095
	std	0.0105	0.0154	0.0283	0.0145	0.0071	0.0065	0.0080
Eight objective (NE = 170000)								
NSGA-II	M-HV	0.0168	0.0000	**0.4947**	**0.8850**	0.8193	0.7068	0.4062
	std	0.0355	0.0000	0.0576	0.0068	0.0068	0.0487	0.0754
DI-MOEA	M-HV	0.0000	0.0000	**0.4250**	**0.9002**	0.8011	0.4619	0.0138
	std	0.0000	0.0000	0.1260	0.0033	0.0196	0.1500	0.0516
NSGA-III	M-HV	0.8543	0.0000	0.3151	**0.9079**	0.8727	0.8632	0.8522
	std	0.0121	0.0000	0.0643	0.0044	0.0074	0.0078	0.0138
NSGA-II	M-IGD	1.2941	2.4798	**0.7887**	0.5247	**0.3955**	0.4332	0.6433
	std	0.1867	0.0422	0.0507	0.0210	0.0068	0.0201	0.0687
DI-MOEA	M-IGD	2.4722	2.5704	**0.8728**	0.4483	**0.4425**	0.6013	2.3017
	std	0.0430	0.0129	0.1118	0.0054	0.0088	0.0682	0.4257
NSGA-III	M-IGD	0.4594	1.9278	0.9662	0.4936	0.4659	0.4638	0.4680
	std	0.0105	0.1043	0.0491	0.0130	0.0099	0.0093	0.0175
Eight objective - Half budget (NE = 85000)								
NSGA-II	M-HV	0.0001	0.0000	**0.4674**	**0.8859**	0.8161	0.7145	0.4251
	std	0.0003	0.0000	0.0847	0.0047	0.0083	0.0334	0.0851
DI-MOEA	M-HV	0.0000	0.0000	**0.4196**	**0.9000**	0.8061	0.5432	0.0213
	std	0.0000	0.0000	0.1254	0.0050	0.0207	0.0931	0.0606
NSGA-III	M-HV	0.8526	0.0000	0.3223	**0.9063**	0.8728	0.8616	0.8548
	std	0.0084	0.0000	0.0553	0.0048	0.0054	0.0085	0.0116
NSGA-II	M-IGD	1.6856	2.4963	**0.8125**	0.5167	**0.3939**	0.4295	0.6116
	std	0.1949	0.0202	0.0763	0.0091	0.0060	0.0126	0.0869
DI-MOEA	M-IGD	2.4858	2.5688	**0.8765**	0.4520	**0.4391**	0.5633	2.0740
	std	0.0272	0.0276	0.1149	0.0073	0.0072	0.0403	0.5132
NSGA-III	M-IGD	0.4611	1.9307	0.9590	0.4923	0.4691	0.4630	**0.4597**
	std	0.0178	0.1646	0.0433	0.0127	0.0115	0.0101	0.0152

Table 3.10: The mean hypervolume (M-HV) and mean IGD (M-IGD) on DTLZ2_convex.

Algorithms	Metrics	P_cone	30°	20°	15°	10°	6°	3°
Four objective (NE = 130000)								
NSGA-II	M-HV	0.4433	0.2126	0.4302	**0.4613**	**0.4577**	**0.4514**	**0.4502**
	std	0.0046	0.0286	0.0025	0.0019	0.0027	0.0037	0.0036
DI-MOEA	M-HV	0.4643	0.0427	0.4308	**0.4673**	**0.4730**	**0.4688**	**0.4678**
	std	0.0071	0.0048	0.0039	0.0051	0.0017	0.0025	0.0019
NSGA-III	M-HV	0.4419	0.1978	0.4182	**0.4501**	**0.4552**	**0.4499**	**0.4470**
	std	0.0078	0.0329	0.0037	0.0036	0.0025	0.0053	0.0036
NSGA-II	M-IGD	0.1484	0.5018	0.2137	0.1512	**0.1454**	**0.1466**	**0.1458**
	std	0.0044	0.0444	0.0036	0.0026	0.0037	0.0046	0.0034
DI-MOEA	M-IGD	0.1284	0.7288	0.2108	0.1426	**0.1238**	**0.1252**	**0.1255**
	std	0.0093	0.0154	0.0055	0.0074	0.0017	0.0034	0.0026
NSGA-III	M-IGD	0.1471	0.5242	0.2295	0.1660	**0.1424**	**0.1439**	**0.1424**
	std	0.0094	0.0511	0.0052	0.0052	0.0031	0.0067	0.0043
Six objective (NE = 150000)								
NSGA-II	M-HV	0.1299	0.0223	**0.1304**	**0.1471**	0.1376	0.1348	0.1325
	std	0.0029	0.0042	0.0016	0.0017	0.0018	0.0027	0.0023
DI-MOEA	M-HV	0.1343	0.0133	0.1280	**0.1525**	0.1408	0.1376	0.1365
	std	0.0018	0.0009	0.0019	0.0011	0.0014	0.0017	0.0020
NSGA-III	M-HV	0.0993	0.0072	**0.1109**	**0.1386**	0.1234	0.1116	0.1045
	std	0.0078	0.0010	0.0026	0.0027	0.0045	0.0061	0.0072
NSGA-II	M-IGD	0.2713	0.5058	0.4106	0.2789	**0.2655**	0.2686	0.2698
	std	0.0047	0.0282	0.0043	0.0049	0.0046	0.0053	0.0054
DI-MOEA	M-IGD	0.2571	0.6012	0.4149	0.2657	**0.2513**	0.2530	0.2557
	std	0.0030	0.0044	0.0050	0.0054	0.0038	0.0029	0.0028
NSGA-III	M-IGD	0.2911	0.7106	0.4557	0.3039	**0.2677**	0.2764	0.2869
	std	0.0093	0.0245	0.0074	0.0110	0.0106	0.0070	0.0073
Eight objective (NE = 170000)								
NSGA-II	M-HV	0.0276	0.0155	0.0187	**0.0355**	0.0298	0.0292	0.0283
	std	0.0010	0.0013	0.0029	0.0005	0.0011	0.0007	0.0008
DI-MOEA	M-HV	0.0264	0.0213	0.0151	**0.0357**	0.0280	0.0269	0.0267
	std	0.0008	0.0007	0.0004	0.0005	0.0006	0.0007	0.0009
NSGA-III	M-HV	0.0210	0.0014	0.0127	**0.0256**	0.0219	0.0211	0.0206
	std	0.0010	0.0013	0.0005	0.0009	0.0015	0.0010	0.0014
NSGA-II	M-IGD	0.3649	0.4218	0.5285	**0.3607**	**0.3548**	0.3573	0.3607
	std	0.0087	0.0083	0.0236	0.0040	0.0061	0.0086	0.0067
DI-MOEA	M-IGD	0.3816	0.3946	0.5611	**0.3597**	0.3736	0.3788	0.3803
	std	0.0036	0.0047	0.0029	0.0048	0.0044	0.0057	0.0050
NSGA-III	M-IGD	0.4197	0.7074	0.5811	**0.4178**	**0.4176**	0.4198	0.4211
	std	0.0094	0.0272	0.0037	0.0073	0.0136	0.0095	0.0120
Eight objective - Half budget (NE = 85000)								
NSGA-II	M-HV	0.0282	0.0152	0.0187	**0.0356**	0.0304	0.0293	0.0286
	std	0.0007	0.0012	0.0025	0.0006	0.0006	0.0007	0.0010
DI-MOEA	M-HV	0.0263	0.0217	0.0150	**0.0359**	0.0276	0.0268	0.0266
	std	0.0010	0.0008	0.0005	0.0006	0.0006	0.0007	0.0008
NSGA-III	M-HV	0.0202	0.0012	0.0126	**0.0249**	0.0213	0.0207	0.0200
	std	0.0013	0.0009	0.0005	0.0009	0.0008	0.0010	0.0014
NSGA-II	M-IGD	0.3649	0.4218	0.5285	**0.3607**	**0.3548**	0.3573	0.3607
	std	0.0087	0.0083	0.0236	0.0040	0.0061	0.0086	0.0067
DI-MOEA	M-IGD	0.3801	0.3937	0.5616	**0.3588**	0.3784	0.3796	0.3792
	std	0.0071	0.0046	0.0037	0.0039	0.0065	0.0074	0.0035
NSGA-III	M-IGD	0.4263	0.7102	0.5815	**0.4210**	0.4238	0.4234	0.4250
	std	0.0113	0.0213	0.0042	0.0093	0.0086	0.0086	0.0110

Table 3.11: The mean hypervolume (M-HV) and mean IGD (M-IGD) on UF11 & UF13.

| Algorithms	Metrics	P_cone	30°	20°	15°	10°	6°	3°
UF11 Five objective (NE = 300000)								
NSGA-II	M-HV	0.0000	0.0000	**0.0211**	**0.0291**	**0.0306**	**0.0218**	**0.0104**
	std	0.0000	0.0000	0.0024	0.0058	0.0012	0.0011	0.0014
DI-MOEA	M-HV	0.0029	0.0000	**0.0191**	**0.0336**	0.0256	0.0188	0.0138
	std	0.0018	0.0000	0.0035	0.0008	0.0012	0.0015	0.0024
NSGA-III	M-HV	0.0147	0.0000	**0.0266**	**0.0350**	0.0278	0.0201	0.0171
	std	0.0016	0.0000	0.0034	0.0017	0.0016	0.0014	0.0015
NSGA-II	M-IGD	1.5208	14.6626	**0.3890**	**0.2990**	**0.2685**	**0.3119**	**0.4531**
	std	0.2173	0.2878	0.0368	0.0374	0.0171	0.0241	0.0289
DI-MOEA	M-IGD	0.7304	15.1690	**0.6152**	**0.2807**	0.3339	0.3946	0.4621
	std	0.0944	0.2054	0.1997	0.0210	0.0228	0.0352	0.0545
NSGA-III	M-IGD	0.4517	15.0785	**0.4190**	**0.2795**	0.3188	0.3848	0.4166
	std	0.0388	0.2105	0.0697	0.0247	0.0235	0.0324	0.0183
UF11 Five objective - Half budget (NE = 150000)								
NSGA-II	M-HV	0.0000	0.0000	**0.0205**	**0.0269**	**0.0288**	**0.0201**	**0.0082**
	std	0.0000	0.0000	0.0025	0.0055	0.0014	0.0016	0.0017
DI-MOEA	M-HV	0.0012	0.0000	**0.0237**	**0.0316**	0.0244	0.0185	0.0126
	std	0.0011	0.0000	0.0030	0.0020	0.0010	0.0014	0.0017
NSGA-III	M-HV	0.0148	0.0000	**0.0268**	**0.0342**	0.0270	0.0199	0.0170
	std	0.0020	0.0000	0.0029	0.0013	0.0018	0.0016	0.0010
NSGA-II	M-IGD	1.7202	14.7243	**0.3951**	**0.3031**	**0.2731**	**0.3208**	**0.4846**
	std	0.2541	0.1769	0.0392	0.0343	0.0164	0.0289	0.0312
DI-MOEA	M-IGD	0.8730	15.1172	**0.4910**	**0.2939**	0.3418	0.4061	0.4831
	std	0.1485	0.2099	0.0619	0.0269	0.0244	0.0329	0.0439
NSGA-III	M-IGD	0.4606	15.0148	**0.3897**	**0.2752**	0.3204	0.4009	0.4314
	std	0.0433	0.1881	0.0615	0.0186	0.0265	0.0393	0.0335
UF13 Five objective (NE = 300000)								
NSGA-II	M-HV	0.6937	0.5041	**0.7410**	**0.7424**	0.7177	0.7065	0.6994
	std	0.0079	0.1742	0.0096	0.0070	0.0091	0.0084	0.0084
DI-MOEA	M-HV	0.6611	0.4625	**0.7343**	**0.7152**	0.6590	0.6567	0.6589
	std	0.0063	0.1580	0.0064	0.0119	0.0073	0.0067	0.0071
NSGA-III	M-HV	0.6498	0.4523	**0.7164**	**0.7226**	0.7023	0.6703	0.6532
	std	0.0130	0.1017	0.0048	0.0108	0.0085	0.0106	0.0077
NSGA-II	M-IGD	1.4761	**1.3108**	1.4316	**1.3805**	1.4656	1.4391	1.4181
	std	0.1315	0.2267	0.0565	0.0857	0.0664	0.1572	0.1029
DI-MOEA	M-IGD	1.5448	**1.5031**	1.5151	1.5481	1.7512	1.6351	1.5934
	std	0.0473	0.4180	0.0533	0.0646	0.0384	0.0667	0.0399
NSGA-III	M-IGD	1.8698	**1.6030**	1.6324	**1.5813**	1.6675	1.7950	1.8527
	std	0.1842	0.1835	0.0285	0.0658	0.0969	0.1457	0.1245
UF13 Five objective - Half budget (NE = 150000)								
NSGA-II	M-HV	0.6687	0.5016	**0.7259**	**0.7170**	0.6915	0.6831	0.6738
	std	0.0041	0.1749	0.0092	0.0058	0.0042	0.0047	0.0057
DI-MOEA	M-HV	0.6457	0.3427	**0.7254**	**0.7002**	0.6513	0.6481	0.6497
	std	0.0045	0.2041	0.0044	0.0133	0.0056	0.0053	0.0057
NSGA-III	M-HV	0.6432	0.4702	**0.7073**	**0.7045**	0.6770	0.6579	0.6417
	std	0.0086	0.0996	0.0074	0.0076	0.0103	0.0071	0.0056
NSGA-II	M-IGD	1.5720	1.3736	**1.5455**	**1.5074**	1.5968	1.5746	**1.5262**
	std	0.0946	0.1703	0.0638	0.0649	0.0786	0.1135	0.0860
DI-MOEA	M-IGD	1.6609	**1.5321**	1.5939	1.6311	1.8048	1.7286	1.6403
	std	0.0557	0.3781	0.0268	0.0781	0.0509	0.0794	0.0613
NSGA-III	M-IGD	1.8931	1.7553	**1.6824**	1.6832	1.8163	1.8976	1.9725
	std	0.1238	0.2361	0.0456	0.0376	0.0924	0.1200	0.0562
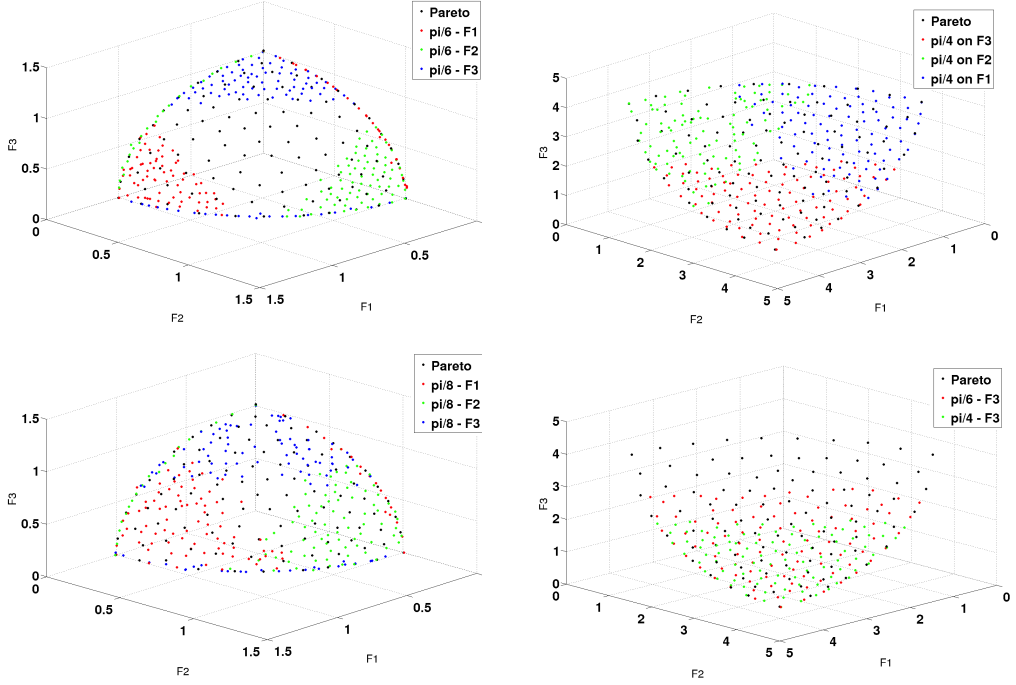
Figure 3.9: Pareto front approximations of (concave & convex) DTLZ2 obtained by the cone with different rotation angles on different edges.

from original DI-MOEA. The blue, green and red points in the top image show the results when only $F3$, $F2$, $F1$ of the standard Pareto cone is rotated outside by $30°$ ($\pi/6$) respectively and the other two edges of the cone remain. In the bottom image, the rotation angle is $22.5°$ ($\pi/8$) on the extended edge and the other edges are the same as those of the Pareto cone. Under the condition that the original Pareto front is concave, it can be observed that the achieved Pareto front focuses on a different corner and the side right against the corner of the entire Pareto front when only one edge of the cone is rotated. Moreover, the smaller the angle, the larger the covered Pareto front area. The right two images in Figure 3.9 present the results on the convex DTLZ2 problem. The points with different colors in the top image, again, show the Pareto fronts when only one edge of the cone is rotated and the rotation angle is $45°$ ($\pi/4$). It can be seen that the solutions focus on different corners. The bottom image shows again when the rotation angle is larger, the Pareto front can be narrowed down and concentrate more on the corner. The literature of the preference-based MOEAs mostly focus on the knee or central region of the Pareto front, however, the edge-

rotated cones make it possible to obtain preferred solutions if the "corner" regions are interested, i.e., the edges of the cone are rotated by different angles to express the preference on different objectives.

3.2.5 Conclusion and Future Work

The edge-rotated cone is generated by simply rotating the edges of the Pareto cone. The edge-rotated cone order, when used as the ranking criterion by MOEAs, can rank the Pareto incomparable solutions into different layers. Hence, the selection pressure toward the Pareto front can be strengthened and the convergence of the algorithm can be accelerated. To avoid neglecting the diversity, the edge-rotated cone order is designed to work together with the standard Pareto order in MOEAs. After testing the edge-rotated cones with various rotation angles on multi-objective and many-objective optimization problems and comparing their performance with the original MOEAs, it can be seen that many-objective optimization can really benefit from the edge-rotated cones. To be specific, a cone with a relatively small rotation angle ($> 3°$, e.g., $6°$) can almost always improve the performance of original algorithms. On many-objective optimization problems, the best behavior usually appears when an intermediate rotation angle (e.g., $15°$) is adopted. However, on multi-objective problems, the rotation angles which can achieve the best performance are usually smaller. In the experiment, it can also be observed that the performance of NSGA-II integrating the edge-rotated cone can reach the performance of NSGA-III in some cases. Moreover, when the algorithm uses a small computing budget and edge-rotated cones, it can achieve better behavior than when the algorithm uses a large budget but without edge-rotated cones.

From the experimental results, it can be seen that a smaller rotation angle is more suitable in low dimensions than in high dimensions. The reason is high dimensional problems need strong convergence. Otherwise, it is difficult to find a good Pareto front approximation. Therefore, a larger rotation angle is needed by many-objective problems. However, a larger rotation angle also leads to the focus of the search on a smaller region of the Pareto front (Please refer to Figure 3.9), MOEAs then need to find a good balance between the convergence and coverage to avoid that the obtained solution set covers only a part of region of the Pareto front. It has also been found that the properties of the problem determine the performance of a specific rotation angle more than the objective number. For example, the rotation angle which can achieve the best performance on DTLZ1 problems is always higher than on other problems, no matter the number of objectives is three, four or eight, and no matter whether the

edge-rotated cone is integrated in NSGA-II or NSGA-III. The reason behind this is that the Pareto front of DTLZ1 problems is linear. All points on the linear Pareto front can be found even when the rotation angle is large. Therefore, a large rotation angle can be used to improve the convergence ability of MOEAs without deteriorating the coverage of the Pareto front. However, when the Pareto front is non-linear, it is possible that only a part of the Pareto front can be obtained by a large rotation angle. In future, the mechanism that relates the properties of the problem with the rotation angle should be researched more. Furthermore, when the edges of the Pareto cone are rotated by different angles, the obtained Pareto front approximation can focus on the different region of the entire Pareto front, and these "unsymmetrical" cones are very promising to be used when exists different emphasis on the Pareto front. However, further research on its ability on articulating the preference on both multi-objective and many-objective optimization should be done. In general, the use of cone orders to formulate preferences based on trade-off rates and angles will be a topic that deserves also attention for problems with a larger number of objectives and tools to better guide users in choosing their preferences will be of crucial importance to improve applicability in practice.